Switching Ti Valence in $SrTiO_3$ by a dc Electric Field

T. Leisegang,[1,*] H. Stöcker,[1] A. A. Levin,[1] T. Weißbach,[1] M. Zschornak,[1] E. Gutmann,[1] K. Rickers,[2] S. Gemming,[3] and D. C. Meyer[1]

[1]*Institut für Strukturphysik, Technische Universität Dresden, 01062 Dresden, Germany*

[2]*Hamburger Synchrotronstrahlungslabor HASYLAB am Deutschen Elektronen-Synchrotron DESY, Notkestrasse 85, 22603 Hamburg, Germany*

[3]*Institut für Ionenstrahlphysik und Materialforschung, Forschungszentrum Dresden-Rossendorf, 01314 Dresden, Germany*

(Received 8 May 2008; revised manuscript received 19 December 2008; published 23 February 2009)

A (001) $SrTiO_3$ wafer has been investigated *in situ* at room temperature under application of a static electric field of varying polarity by fluorescence x-ray absorption near edge structure (XANES) analysis at the Sr-*K* and Ti-*K* absorption edges. The XANES spectra show a clear shift of the Ti-*K* absorption edge energy. The shift is attributed to a change of the Ti valence state in a volume invoked by diffusion of the oxygen ions and vacancies. No shift was observed for the Sr-*K* absorption edge energy. Theoretical calculations support these findings.

DOI: 10.1103/PhysRevLett.102.087601 PACS numbers: 77.84.Bw, 61.05.cj, 66.30.Qa, 71.55.−i

During the last decade, extensive investigations have focused on ferroelectric, ferromagnetic, and ferroelastic materials [1]. Their ferroic properties arise from a spontaneous long-range ordering of, e.g., electric dipoles or magnetic moments or strained orientation domains. Important characteristics of these materials are, e.g., high dielectric constants, piezo- or pyroelectricity or giant magnetoresistance. A coupling of at least two ferroic properties, named multiferroicity, allows for a large diversity of upcoming applications, e.g., microelectromechanical systems, magnetoelectric transducers, microwave electronics, ferroelectric field effect transistors, as well as data storage and random access memory devices [1–4].

Among ferroic or multiferroic materials, oxides with perovskite-type structure have gained great importance. To maintain structural integrity, they are mostly grown epitaxially. $SrTiO_3$ (STO) is widely used as a substrate material due to its compatible lattice parameters, structure, and comparatively low chemical reactivity [3]. Pristine STO is characterized by a perovskite-type cubic structure [lattice parameter $a_0 = 3.905$ Å at room temperature (RT)] [5] and exhibits no crystallographic phase transitions down to a temperature of ~105 K and no ferro- or piezoelectric behavior down to helium temperatures [6].

The growth as well as processing of oxide single crystals, such as STO, introduces a specific density of Schottky point defects. Although several defect reducing approaches are utilized, in particular, near-surface regions still exhibit a distorted structure [3,7]. Essentially oxygen vacancies, introducing lattice distortions and charge carriers, show a strong impact on structural and electronic properties, e.g., phase transitions, ionic conductivity, and resistance switching [8,9].

In comparison with the ideal crystal structure, a statistical distribution of oxygen vacancies in STO results in an expansion of the average cubic unit cell [10]. However, they can also arrange periodically forming linear or planar defects causing the formation of intergrowth structures [11]. Hence, specific well-defined oxygen-deficient tetragonal phases, i.e., $SrTiO_{3-\delta}$ and $SrTi_{1-x}O_{3-y}$ [$x = 1/(n+1)$, $y = 2/(n+1)$, $n = 1, 2, \ldots$], can be formed [12,13].

Application of a static (dc) electric field to a STO crystal results in a redistribution of oxygen vacancies and subsequently in structural changes. Early experiments revealed ionic conductivity in STO and the influence of a dc electric field thereon [14]. It has been suggested that either oxygen vacancies or SrO complexes gain an enhanced diffusion coefficient when transported along dislocation lines or planar defects [9,15]. Recently, for (001) STO wafers we have found a reversible change of the x-ray reflection profiles using wide-angle x-ray diffraction under application of a dc electric field at RT [16]. This phenomenon has been attributed to structural variations observed beneath the anode (usually at the as-cut unpolished side) and promises application in the field of adaptive x-ray optics [17].

In the present report we focus on the characterization of the near-surface structure of STO under the influence of an electric field. We performed dedicated fluorescence x-ray absorption near edge structure (XANES) investigations at the Sr-*K* and Ti-*K* absorption edge of a (001) STO single-crystal plate (supplied by Crystec GmbH, Germany, etched with NH_4F buffered HF) at RT *in situ* under the influence of a dc electric field. The measurements were carried out at beam line C (CEMO) [18] of the Hamburger Synchrotronstrahlungslabor (HASYLAB) at Deutsches Elektronen-Synchrotron (DESY) using grazing incidence of the exciting x rays. This experiment allows investigating changes of the valence states of the Sr and Ti atoms based on the binding energy of the resonantly excited $1s$ *K*-shell electrons. The STO crystal plate (size $10 \times 10 \times 0.5$ mm^3) used for this experiment was coated with W electrodes (thickness $t \approx 70$ nm) on top of B_4C diffusion barriers

($t \approx 30$ nm) on both sides of the plate, so that a voltage of $U = \pm 500$ V, corresponding to an electric field strength of $E_z = \pm 10^6$ V/m, could be applied (see Fig. 1). The electric field was applied for 115 min ($U = +500$ V) and 19 min ($U = -500$ V) in case of the Ti and at least 3 times longer in case of the Sr-K XANES measurements. The voltage source used (Physik Instrumente E-507) ensured a constant voltage and thus a constant electric field over time. The electric current through the sample, monitored throughout the whole experiment, increased generally but remained below 10^{-7} A. A detailed description of the behavior of the electric current will be given elsewhere.

The XANES spectra were collected repeatedly using a fixed-exit Si (111) double crystal monochromator [19] for an energy range of the exciting photons of $E = 16\,000 \ldots 16\,150$ eV and $E = 4960 \ldots 5000$ eV (Sr-K and Ti-K absorption edge) with an energy step width of $\Delta E = 0.5$ eV and $\Delta E = 1$ eV, respectively. An angle of incidence $\omega = 0.15°$ was chosen to probe the distorted near-surface region (attenuation depth of about 200 and 20 nm for Sr-K and Ti-K edge energies of x-ray radiation, respectively) with most significance. An energy resolving solid state detector (Kevex PSI) was arranged perpendicular to the plane of scattering so that the fluorescence yield I_F could be collected in the direction of the polarization vector of the synchrotron radiation enhancing the signal-to-noise ratio. XANES spectra were obtained by integration of the fluorescence spectra over energy ranges of interest (ROI) 13.3...15.3 keV (Sr-$K\alpha$) and 4.3...5.0 keV (Ti-$K\alpha$), respectively, and normalization relative to the primary beam intensity. Calibration of the energy scale was done by testing absorption edge energies of several metal foils. The exciting photons were guided through an evacuated ($p < 10^{-6}$ mbar) beam guide. Three different XANES spectra were recorded, one in zero-electric field and two during application of the electric field with different polarity. After every change of the electric field strength, a realignment procedure was performed to correct for height and tilt changes of the irradiated sample surface, both caused by the electric field [20].

For the investigated side, the *in situ* XANES spectra exhibited no differences within the estimated error in the case of the Sr-K absorption edge [Fig. 2(a)] indicating an unchanged or at most marginally affected valence state of the Sr atoms under the influence of the electric field applied. In case of the Ti atoms a significant shift of the Ti-K absorption edge energy (determined by the maximum of first derivative of $I_{F,\mathrm{norm}}(E)$ which was fitted with a Gaussian profile) of (1.29 ± 0.06) eV due to the electric field was observed [Fig. 2(b)]. In particular, the voltage applied to the sample surface increased ($U = +500$ V) or decreased ($U = -500$ V) the Ti-K absorption edge energy within the crystal volume probed in the experiment. In case of a positive voltage the Ti-K absorption edge energy shifted to higher values over time with a rate of (0.005 ± 0.001) eV/min. Within the time period investigated (115 min) no plateau was observed. The short duration of the electric field application with negative voltage (19 min) did not allow elucidating the time dependence.

A rather qualitative interpretation of the results can be drawn in terms of ionic conductivity. The near-surface

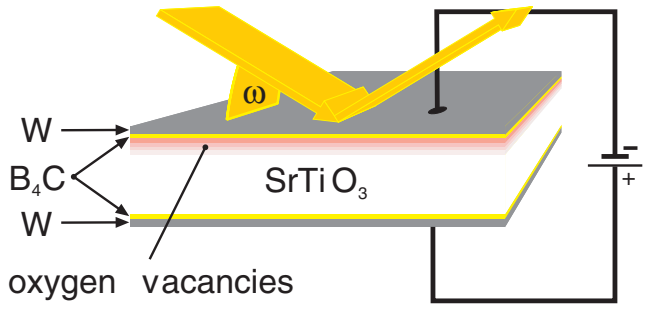

FIG. 1 (color online). Schematic representation of the experimental setup with incident angle ω of the exciting x rays.

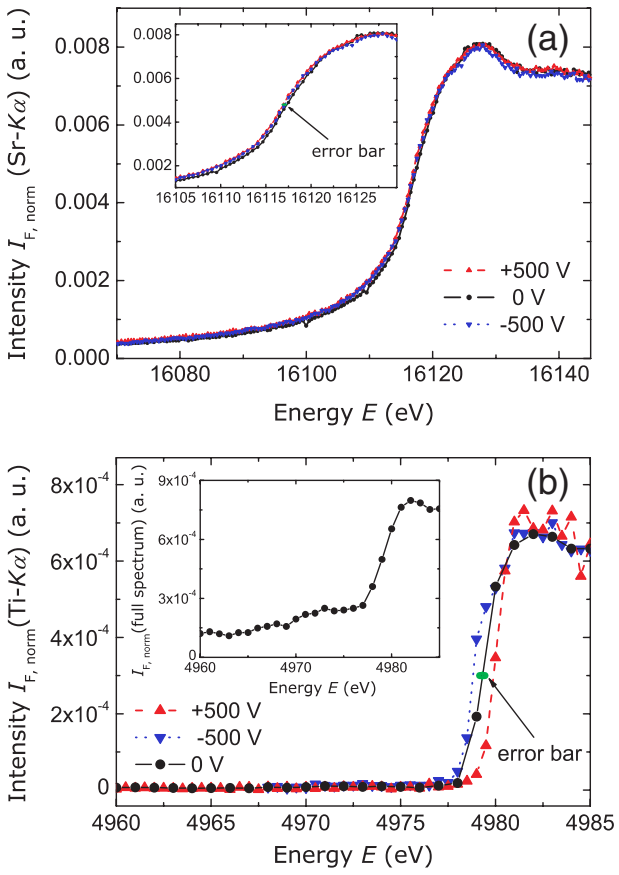

FIG. 2 (color online). XANES spectra for photon energies at (a) the Sr-K and (b) the Ti-K (ROI: 4.3...5.0 keV) absorption edges under application of a dc electric field. The inset in (a) gives an enlarged view of the Sr-K absorption edge region. An exemplary XANES spectrum for the completely integrated energy range (ROI: 3.1...8.5 keV) of the fluorescence yield showing the well-known preedge features of Ti is depicted in the inset of (b).

region of the unpolished STO plate is considered to contain an increased amount of oxygen vacancies. By applying a voltage of positive polarity to this distorted surface, oxygen is forced to migrate from the bulk to the anode so that it compensates the intrinsic oxygen vacancies at the irradiated near-surface region. Thereby, the coordination of Ti atoms changes from square-planar or pyramidal (in case of oxygen vacancy) to octahedral symmetry, the formal Ti valence state shifts from $Ti^{(4-\delta)+}$ next to a vacancy back to Ti^{4+} and the ideal STO structure is recovered in the near-surface volume probed. Thus, the shift of the Ti-K absorption edge energy to a higher value in Fig. 2(b) can be attributed to a filling of oxygen vacancies by oxygen diffusion mediated by the electric field.

Inversion of the polarity ($U = -500$ V), i.e., the near-surface region acts as cathode, reverses the oxygen anion transport and the Ti-K absorption edge energy decreases, implying a change of the formal oxidation state from Ti^{4+} to $Ti^{(4-\delta)+}$ [Fig. 2(b)]. The final state at the cathode indicates that the Ti-K absorption edge energy is shifted to energies lower than that observed for the state without an electric field. Consequently, more oxygen atoms diffuse into the bulk material thereby increasing the density of near-surface vacancies. Referring to previous investigations planar and line defects are assumed to be the most significant diffusion paths [9,15,17,21].

Comparing the shift of the Ti-K absorption edge energy with literature data on various Ti containing compounds with different Ti oxidation states (shift of 3.83 eV between formal Ti^{3+} and Ti^{4+}) [22], we can note that our data are consistent with a change of the Ti valence state. In addition, the form of the XANES spectra at the Ti-K absorption edge also depends on structural disorder. Comparing the white line region of the graphs in Fig. 2(b) with the recently reported spectra in Refs. [23–25] we can state that our model is consistent with a highly crystalline surface in case of positive voltage and with a comparatively more perturbed surface for negative voltage.

The well-known Ti preedge features are visualized by using the completely integrated fluorescence spectra [ROI: 3.1...8.5 keV, inset of Fig. 2(b)]. However, because of a low signal-to-noise ratio, these data do not allow for interpretation of changes of XANES spectra induced by application of the electric field. Therefore, the limited data (ROI: 4.3...5.0 keV for Ti-$K\alpha$) were used for analysis of the XANES spectra described above. By using a limited integrated spectral range, preedge features can disappear [26] as was observed here [Fig. 2(b)].

In the following we substantiate the qualitative suggestions with a more quantitative approach. Low-lying core states such as the Ti 1s state can be employed as local probe for the chemical potential in the vicinity of a given site. Shifts of such levels are commonly related to changes of the local crystal potential due to changes of the coordination geometry or the formal oxidation state [27]. Core-level shifts are also accessible by all-electron density-functional calculations and changes of ionization energies can be obtained and interpreted with this methodology [28,29].

Here, we model the influence of neutral oxygen vacancies V_O on the Ti 1s core level by scalar-relativistic all-electron local-spin-density-functional (LSDA + U) calculations with the FPLO-5 code [30]. A supercell with four $SrTiO_3$ formula units and cell dimensions of $a = b = 2a_0$ and $c = a_0$ was employed and repeated by periodic boundary conditions. An ordered array of oxygen vacancies was simulated by removing one oxygen atom from this supercell (see Fig. 3) resulting in a composition of $SrTiO_{2.75}$; i.e., about 8% of oxygen sites are vacant.

This supercell reproduces the favored chainlike accumulation of oxygen vacancies along a ⟨001⟩ direction obtained in a previous valence-only density-functional study [31]. For the present calculation we adopted all numerical settings according to the values established there [28], especially the on-site Coulomb and exchange terms with an effective parameter $U_{\text{eff}} = 4.46$ eV. In the supercell each vacancy chain and its periodic replica are at least 7.802 Å apart and separated by a volume with ideal bulk-type structure. Three Ti sites can be distinguished in this model: Ti1, the most strongly perturbed, square-planar coordinated neighbor site within the vacancy chain at a distance $d(\text{Ti1-}V_O) = 1.95$ Å and the more distant six-fold coordinated sites Ti2 at $d(\text{Ti2-}V_O) = 4.36$ Å and Ti3 at $d(\text{Ti3-}V_O) = 5.85$ Å. As the calculation does not yield absolute XANES edge onsets, the 1s orbital of the most bulklike Ti3 atom was employed as an internal standard for the Ti 1s core level. We obtained a Ti 1s binding energy reduction of 1.1 eV for the Ti1 atom in the vacancy chain

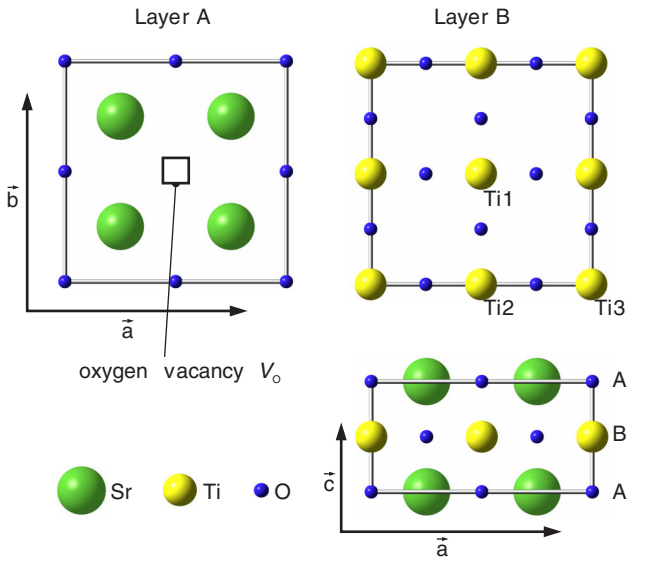

FIG. 3 (color online). Sketch of the supercell used for the LSDA + U calculation. The different Ti environments and the oxygen vacancy are indicated.

and of 0.3 eV for Ti2. These values reflect very well the experimentally observed shift of the Ti-K absorption edge energy and, in particular, the formation of the shoulder-type XANES in the case of $U = -500$ V compared to ideal STO at $U = +500$ V. For the Sr 1s binding energy no prediction can be made because only a unique Sr site was incorporated in our model. Thus, we ascribe the observed Ti-K absorption edge energy shift to the influence of O vacancies on the local electronic structure at the adjacent Ti sites.

In conclusion, XANES measurements proved a shift of the Ti-K absorption edge energy of STO under applied dc electric fields, which has not been reported so far to the best of our knowledge. The results of theoretical calculations show that such shifts of the Ti-K absorption edge energy can be caused by oxygen vacancy redistribution. Taking into account the observed energy shift of the Ti-K absorption edge, a change of vacancy concentration in the order of 8% in the near-surface region was estimated. The Sr-K absorption edge energy, in contrast, is not affected. These investigations provide new insight into the origin of the remarkable changes of the properties occurring in STO in an applied electric field at the atomic scale. Thus, a controlled switching of the Ti valance gives rise to a large variety of interesting applications and physical phenomena, e.g., dedicated valence states for controlled catalytic behavior on STO surfaces or tuning of superconductivity [32] or of insulator-to-metal transition [33].

The authors are indebted to D. Novikov and E. Welter (HASYLAB) for supporting the experiments, DESY for granting beam time and to DFG (research unit FOR 520 and Projects No. ME 1433/4-4, No. GE 1037/9-1, and No. GE 1202/5-1) for financial support.

*leisegang@physik.tu-dresden.de

[1] N. Setter *et al.*, J. Appl. Phys. **100**, 051606 (2006).
[2] K. Dörr and C. Thiele, Phys. Status Solidi B **243**, 21 (2006).
[3] *Physics of Ferroelectrics: A Modern Perspective (Topics in Applied Physics)*, edited by K. Rabe, Ch. H. Ahn, and J.-M. Triscone (Springer, Berlin, 2007), Vol. 105.
[4] S. Gemming *et al.*, J. Comput.-Aided Mater. Des. **14**, 211 (2007).
[5] H. E. Swanson and R. K. Fuyat, Natl. Bur. Stand. Circ. (U.S.) **539**, 44 (1954); ICDD-PDF2, No. 035-0734.
[6] H. Unoki and T. Sakudo, J. Phys. Soc. Jpn. **23**, 546 (1967).
[7] U. Rütt, A. Diedrichs, J. R. Schneider, and G. Shirane, Europhys. Lett. **39**, 395 (1997).
[8] J. P. Buban, H. Iddir, and S. Ogüt, Phys. Rev. B **69**, 180102 (R) (2004).
[9] K. Szot, W. Speier, G. Bihlmayer, and R. Waser, Nature Mater. **5**, 312 (2006).
[10] R. Perez-Casero *et al.*, Phys. Rev. B **75**, 165317 (2007).
[11] L. E. Smart and E. A. Moore, *Solid State Chemistry* (Taylor & Francis, Boca Raton, 2005).
[12] W. Gong *et al.*, J. Solid State Chem. **90**, 320 (1991).
[13] S. N. Ruddlesden and P. Popper, Acta Crystallogr. **11**, 54 (1958).
[14] E. Hegenbarth, Phys. Status Solidi **6**, 333 (1964).
[15] M. Bobeth *et al.*, J. Ceram. Soc. Jpn. **114**, 1029 (2006).
[16] D. C. Meyer *et al.*, Appl. Phys. A **80**, 515 (2005).
[17] D. C. Meyer *et al.*, Appl. Phys. A **84**, 31 (2006).
[18] K. Rickers *et al.*, in *X-Ray Absorption Fine Structure–XAFS13: 13th International Conference on X-Ray Absorption Fine Structure, Stanford, 2006*, edited by Britt Hedman and Piero Pianetta, AIP Conf. Proc. No. 882 (AIP, New York, 2007), p. 905.
[19] K. Rickers *et al.*, in *Proceedings of the 9th International Conference on Synchrotron Radiation Instrumentation, Daegu SRI 2006*, edited by Jae-Young Choi and Seungyu Rah, AIP Conf. Proc. No. 879 (AIP, New York, 2007), p. 907.
[20] T. Leisegang *et al.*, HASYLAB Ann. Rep. **1**, 1109 (2007).
[21] W. T. Lee, E. K. H. Salje, L. Goncalves-Ferreira, M. Daraktchiev, and U. Bismayer, Phys. Rev. B **73**, 214110 (2006).
[22] J. Graetz, J. J. Reilly, J. Johnson, A. Yu. Ignatov, and T. A. Tyson, Appl. Phys. Lett. **85**, 500 (2004).
[23] A. I. Frenkel *et al.*, Phys. Rev. Lett. **99**, 215502 (2007).
[24] C. Sabathier, J. Chaumont, S. Rouziere, and A. Traverse, Nucl. Instrum. Methods Phys. Res., Sect. B **234**, 509 (2005).
[25] F. Farges, G. E. Brown, Jr., and J. J. Rehr, Phys. Rev. B **56**, 1809 (1997).
[26] F. M. F. de Groot, in *X-Ray Absorption Fine Structure–XAFS13* (Ref. [18]), p. 37.
[27] A. Baraldi, J. Phys. Condens. Matter **20**, 093001 (2008).
[28] A. T. Paxton, A. J. Craven, J. M. Gregg, and D. W. McComb, J. Microsc. **210**, 35 (2003).
[29] S. Nufer, T. Gemming, C. Elsässer, S. Köstlmeier, and M. Rühle, Ultramicroscopy **86**, 339 (2001).
[30] K. Koepernik and H. Eschrig, Phys. Rev. B **59**, 1743 (1999).
[31] Do Duc Cuong *et al.*, Phys. Rev. Lett. **98**, 115503 (2007).
[32] J. F. Schooley, W. R. Hosler, and E. Ambler, Phys. Rev. Lett. **12**, 474 (1964).
[33] P. Calvani, M. Capizzi, and F. Donato, Phys. Rev. B **47**, 8917 (1993).